UNITED NATIONS UNIVERSITY
UNU-GTP
Geothermal Training Programme

Orkustofnun, Grensasvegur 9,
IS-108 Reykjavik, Iceland

Reports 2014
Number 22

FEASIBILITY STUDY OF USING A DOWNHOLE PUMPING SYSTEM IN MENENGAI WELL MW-17 FOR GEOTHERMAL UTILIZATION

Hilary Mwangeka Mwawasi
Geothermal Development Company - GDC
P.O. Box 17700-20100
Nakuru
KENYA
hmwawasi@gdc.co.ke, hngeka@yahoo.com

ABSTRACT

Utilization of low to moderate enthalpy fluids for electrical power generation is best carried out using a binary energy conversion system. Several technical variations of the binary cycle exist and include the Kalina cycle and the organic Rankine cycle (ORC). The generation of electrical power using pumped brine from well MW-17 is proposed in this report. The utilization scheme consists of an electrical submersible pump (ESP) of 45 kg/s production capacity and an ORC plant. Detailed calculations and optimization using Engineering Equation Solver (EES) software were carried out and show that an ESP of 700 kW tandem motor power is required. In the present study four working fluids (n-butane, isobutene, n-pentane and isopentane) were considered as possible working fluids in the thermodynamic cycle of the binary power plant created in EES and optimized to obtain optimum net power output. An optimum net power output of 832 kW (0.832 MWe) for a turbine inlet pressure of 7 bar using isopentane was indicated by the EES program runs.

1. INTRODUCTION

Menengai geothermal field development is one of several energy projects being implemented by the government of Kenya as part of its developmental blue print (Vision 2030) that aims at transforming the country into a middle income status economy. The project is being executed on behalf of the government's Ministry of Energy and Petroleum (MoE&P) by Geothermal Development Company Ltd. (GDC). The field is located approximately 180 km northwest of Nairobi and encompasses the Menengai volcano, the Ol' rongai volcanoes, Ol' banita plains and parts of the Solai graben to the northeast, an area measuring approximately 850 km^2 (Mibei and Lagat, 2011) bound by eastings 157000 and 185000 and northings 9966000 and the Equator (Figure 1).

Development of this geothermal resource is being carried out in phases with phase I (Menengai phase I) targeting the realization of enough steam to generate 400 MW (4 x 100) of power (Ngugi, 2012a). This involves drilling an estimated 120 geothermal wells, development of an associated infrastructure, construction of a steam and brine gathering system, environmental management, coordination of project related interface activities (construction of conventional & modular power plants and electricity transmission lines) and integrating direct use applications. GDC intends to avail realized steam (as fuel)

to independent power producers who will run the conventional and modular power generation plants (Ngugi, 2012b).

1.1 Drilling progress at Menengai

Drilling activities began in February 2011 using 2 land rigs (GDC drilling rigs 1 and 2), each with a 2000HP capacity. Three exploration wells, MW-1, MW-2 and MW-3, were drilled in the period from 12th February 2011 to 9th September 2011. Preliminary well test data of Menengai exploration wells, presented by Ofwona et al. (2011), indicated bottom hole temperatures above 300°C and a water rest level at 400 m in the wells. Discharge test results showed a total flow enthalpy of above 1200 kJ/kg for the case of well MW-1. In Suwai (2011), well measurement findings indicated a stabilized maximum total well discharge flow of around 45 kg/s from well MW-1. As of May 2014, production drilling was in progress with a total of 23 wells drilled. The number of land rigs deployed at the project was four (GDC drilling rigs 3 and 4 included) with approximately 80 drilling and support staff accommodated at the Menengai project camp. Well measurements and tests have indicated that hitherto the defined resource area is majorly characterized by high enthalpy dry and two phase steam.

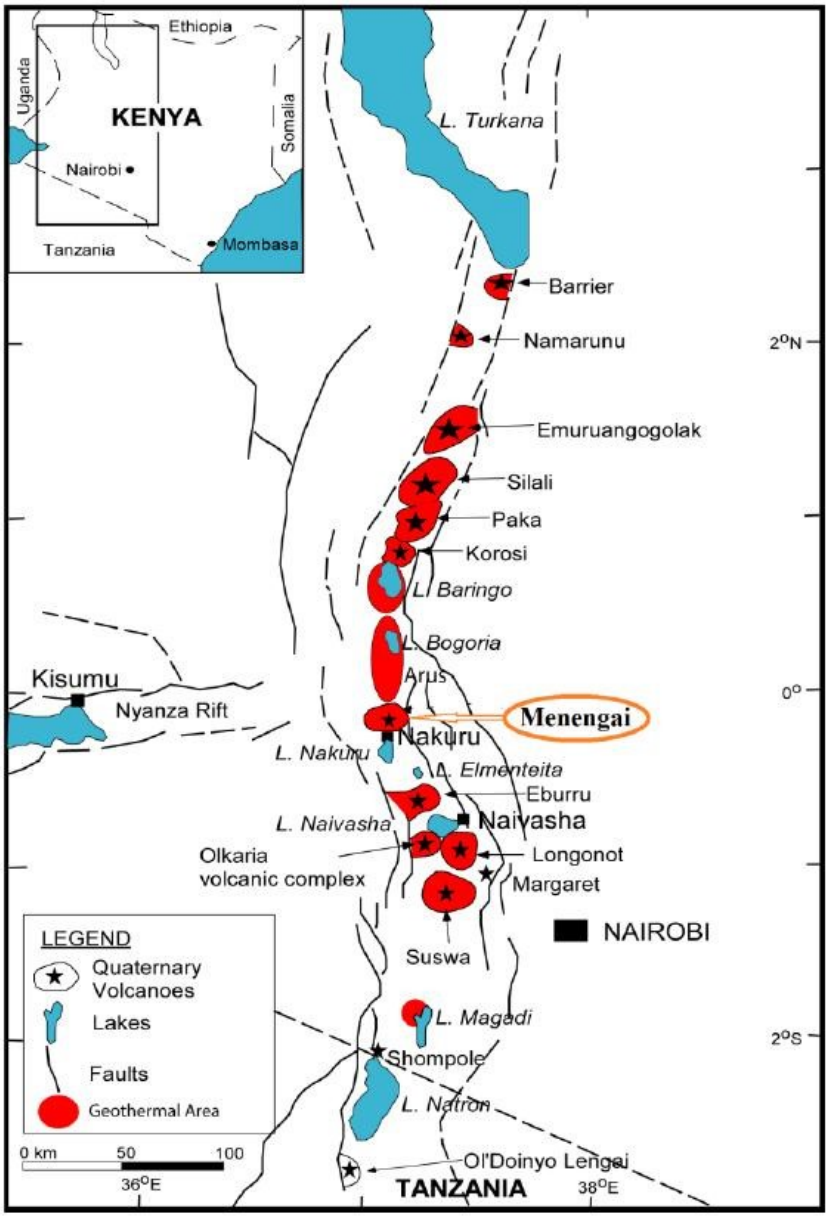

FIGURE 1: Map showing Menengai and other geothermal prospects along the Kenyan Rift Valley

1.2 Candidate well

Two wells were considered for geothermal utilization using a downhole pumping system. Wells MW-5A and MW-17 are located within the Menengai phase I project area.

1.2.1 Well MW-5A

Well MW-5A is located in the southern part of the Menengai caldera, almost immediately past the dome area, and is drilled to a depth of 2084 m. Downhole temperature and pressure profiles for well MW-

5A, attached in Appendix I, indicate the existence of permeable zones at 850, 1150, 1350, 1800 and 2000 m, respectively, and coincide with the occurrence of tuff intercalations and circulation loss zones. An isothermal section is evident in all profiles from the depth interval 1300 to 1800 m; from the hydrostatic pressure profiles, the water level is indicated to be at a depth of 400 m. The maximum bottom hole pressure is about 150 bars.

1.2.2 Well MW-17

This well was drilled in a southwest direction, also within the Menengai caldera. Downhole temperature and pressure profiles are also attached in Appendix I. From temperature profiles, permeable zones can be inferred at intervals 1000-1200 m, 1400-1600 m, 1800-1850 m and at the well bottom. In this well the isothermal section is conspicuous between 1100 and 1850 m, as seen in the heat-up period profiles. Post discharge attempt temperature profiles further indicate that the well has heated up, with the most recent profile indicating a maximum temperature of 175°C at a depth of 1000 m. Pressure profiles indicate a static water rest level that recedes between 445 and 470 m with a wellhead pressure (WHP) of about 130±10 psi (9 bar-g).

Well MW-17 presented a good candidate for generating electrical power using a downhole pump and a binary power plant unit and will be considered for the feasibility study in this report. Figure 2 shows well locations inside the Menengai geothermal field as of May 2014; wells MW-5A and MW-17 are enclosed in red squares.

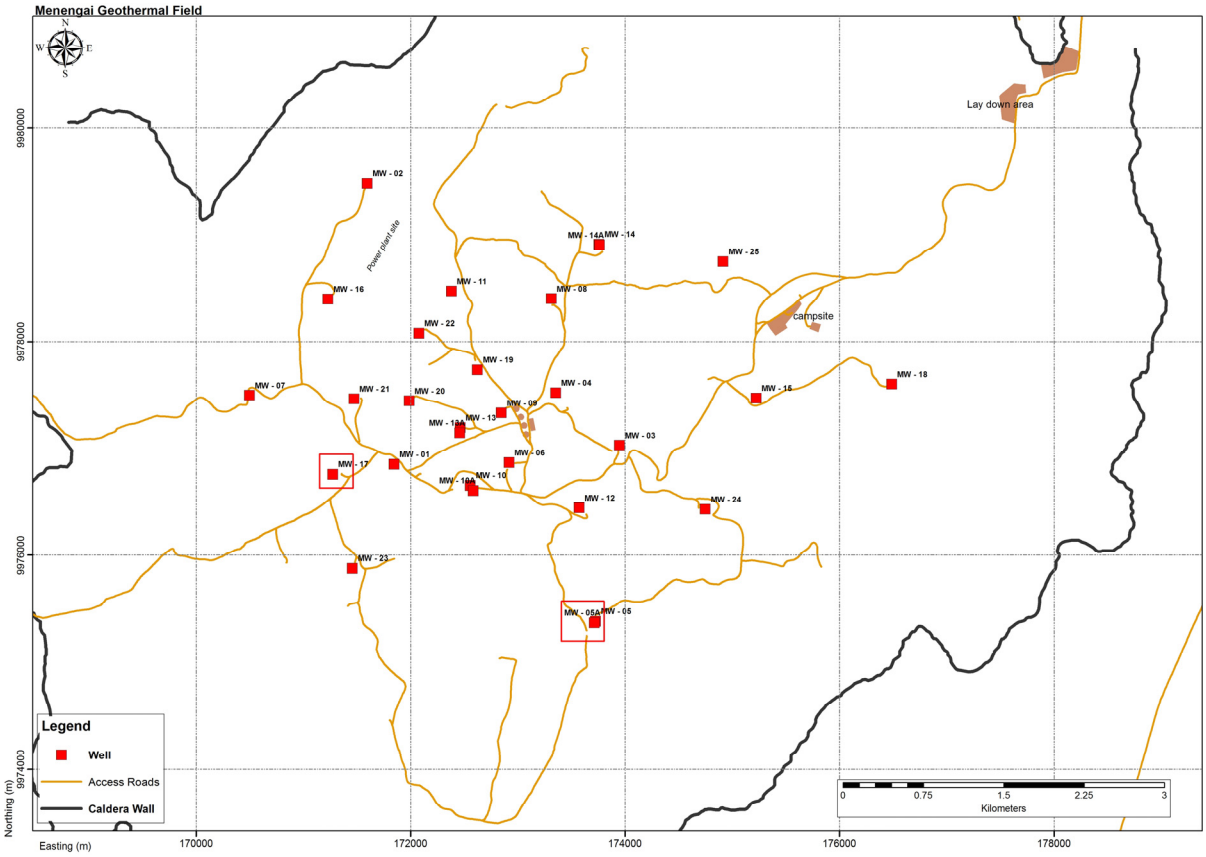

FIGURE 2: Map showing well locations in Menengai geothermal field

1.3 Project scope

This project aims to evaluate the viability of generating electrical power by using a downhole pump in Menengai well MW-17. Results of downhole temperature and pressure measurements for well MW-17 will be reviewed to enable design calculations and the selection of the proper pump system. A suitable combination of a downhole pumping system and a binary power cycle will be identified and the system analysed.

2. WELL FLOW MECHANISM

There are generally two types of well flow mechanisms, self-flowing or artificial lift. Geothermal wells with sufficient reservoir temperature above 190°C can self-flow. Below a temperature of 190°C, artificial lift is more often needed (Sanyal et al., 2007). Utilization of the pumped geothermal fluid for generation of electrical power involves combining the downhole pump system with a suitable power cycle. Technological innovations in the recent past have resulted in improvements in downhole pump resilience to hostile downhole environments, setting depths, gas handling capabilities, resistance to abrasion, performance and reliability.

2.1 Downhole pumps for geothermal wells

Downhole temperature conditions below 190°C are generally associated with medium to high enthalpy liquid phases. Though limited to the operating temperature of the pump, several benefits can be attributed to the use of downhole pumps in geothermal wells as outlined below:

- Greater generating capacity and no reduction in output due to well scaling;
- Increased production from each well, by lowering of water rest level;
- Higher wellhead temperature;
- No loss of steam to the atmosphere; better energy recovery; and
- Reduced calcite scale potential where geothermal fluids with high carbon dioxide content are kept under pressure.

Two types of downhole pumps are commonly used in geothermal wells, line shaft pumps (LSP) and electrical submersible pumps (ESP). The two types are distinguished from each other by the location of the driver. In LSP the driver, an electrical motor, is usually installed above the wellhead (on the surface) and drives the pump through a long shaft. The ESP has the electric motor located below the pump itself and together they are installed inside the wellbore at depth. Figures 3 and 4 give examples of typical LSP and ESP installation concepts.

2.2 Comparison of LSP and ESP

Culver and Rafferty (1998) gave a general comparison of line shaft and electrical submersible pumps as illustrated in Table 1.

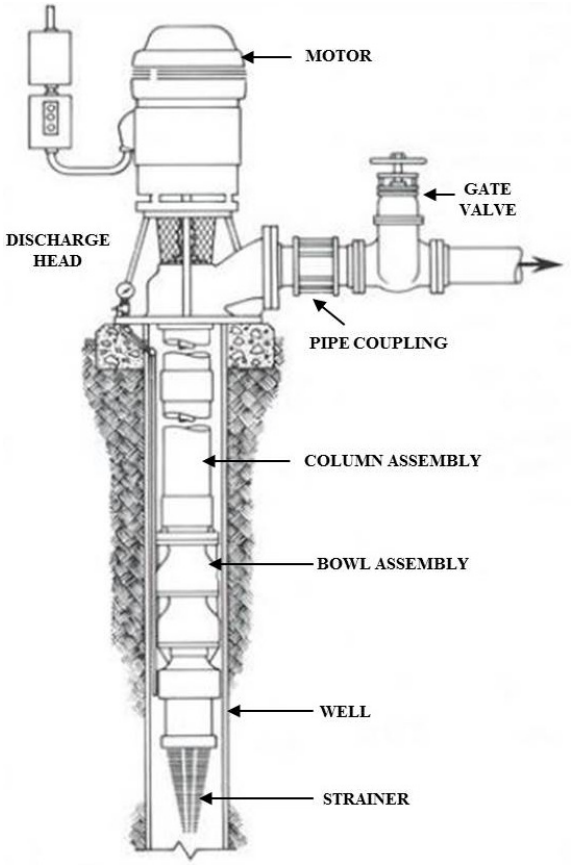

FIGURE 3: Line shaft pump LSP (Kaya and Mertoglu, 2005)

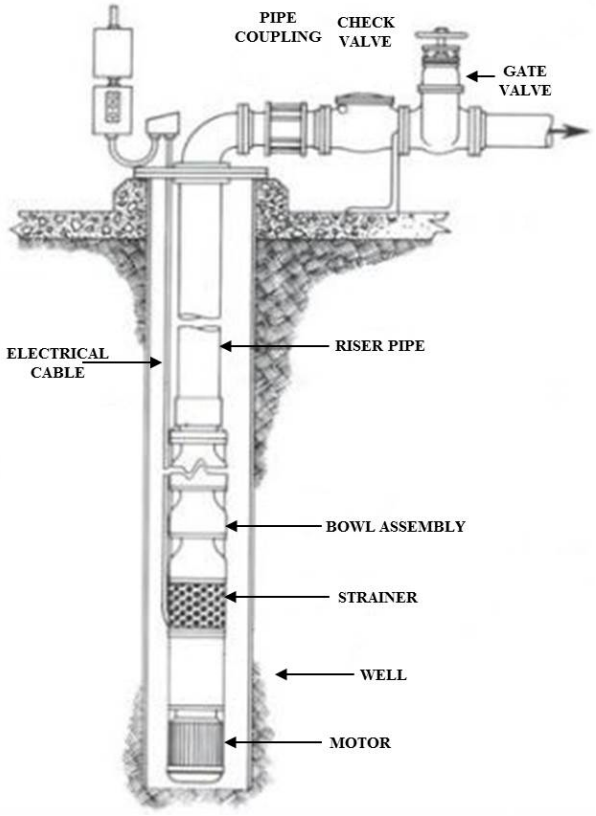

FIGURE 4: Electrical submersible pump ESP (Kaya and Mertoglu, 2005)

TABLE 1: Comparison of line shaft and electrical submersible pumps

Line shaft	Electrical submersible
Pump stage efficiencies in the range 68 – 78%. Lower head/stage and flow/unit diameter.	Pump stage efficiencies in the range 68 -78%. Have generally higher flow/unit diameter.
Higher motor efficiency, motor operates in air, little losses in power cable, and mechanical losses in shaft bearings.	Relatively lower motor efficiency, motor operates in oil at elevated temperatures, higher losses in power cable since partially submerged and attached to hot tubing.
Motor, thrust bearing and seal accessible at surface.	Motor, thrust bearings, seal and power cable in well, hence less accessible.
Usually lower speed (1750 rpm or less), lower wear rate.	Usually higher speeds (3600 rpm), higher wear rate.
Shallower setting, approximately 600 m maximum.	Deeper settings, up to approximately 3,650 m in oil wells.
Longer installation and pump pull time.	Less installation and pump pull time.
Well must be relatively straight or oversized to accommodate stiff pump and column.	Can be installed in crooked wells up to 4 degrees deviation per 100 ft. Up to 75 degrees off vertical.
Impeller position must be adjusted at initial start-up.	Impeller position set.
Generally lower purchase price at direct use temperatures and depth.	Generally higher purchase price at direct use temperatures and depth.

2.3 Downhole pump selection criteria

Selection of a downhole pump has for several installations been based on the following considerations:

- Setting depth;
- Well size;
- Well deviation;
- Well temperature;
- Wire-to-water efficiency;
- Power consumption costs;
- Lowest life cycle costs;
- Repair costs;
- Availability of spare parts; and
- Downtime costs.

These criteria were considered by carrying out a literature review on downhole pump installation experiences in several geothermal projects and published studies as presented in Kunaruk (1991), Ichikawa et al., (2000), Kaya and Mertoglu (2005), Genter et al., (2010), and Drader (2011). The pump setting depth was calculated for various possible flow rates from the well, taking into account the water rest level (L_V), minimum pump submergence (h_{min}) and drawdown in the well (L_N). Drawdown was assumed to be controlled by well losses. Current LSP technology is limited to a setting depth of 457 m (Sanyal et al., 2007); beyond this depth, the pump unit may be affected by vibration or loss of bowl unit efficiency due to the relative elongation between the outer system (column, impeller housings and shaft enclosing tube) and inners system (shaft and impellers). ESP technology has a considerably deeper setting depth and was, thus, determined as the ideal downhole pump for well MW-17.

2.4 ESP analysis and design theory

Similar principles are applicable in calculations for LSP and ESP (Frost, 2004). The design criteria vary depending on the production conditions and well fluid properties anticipated. A model was set up using Engineering Equation Solver (EES) software (F-Chart Software, 2014), based on the following downhole pump design criteria:

- Collection and analysis of available basic data for design, including: well data, production data, well fluid conditions, power sources and possible challenges (temperature, gas fraction, corrosion, deposition);
- Determination of production capacity and pump intake pressure;
- Calculation of the total dynamic head required, expressed in terms of pumped fluid column pressure;
- Selection of a suitable pump unit type based on manufacturer data available, done while ensuring the outer diameter (O.D.) of the pump unit fits inside the casing of the well;
- Calculation of required shaft output power and power consumption; the choice of motor should ensure the motor is large enough to withstand the maximum load without overloading it;
- Selection of the power cable type and size based on motor current, conductor temperature and space limitations; and
- Selection of accessories and optional equipment.

2.5 Basic design data

Well MW-17 was selected for this project. Available data included well casing data, temperature and pressure profiles, material properties and weather data.

2.6 Water rest level in well due to column heating

The static water column in the well gets heated up to pumping conditions. The temperature elevation leads to changes in water density and, consequently, the water rest level in the well. The water rest level in the well, due to heating (L_V), was estimated from the equation:

$$L_V = L_{ref} - L_C \quad (1)$$

where L_V = Water rest level in well due to column heating (m);
L_{ref} = Reference major feed zone (m);
L_C = Water column due to well heating (m).

The water column due to well heating (L_C), is estimated from the equation:

$$L_C = \frac{P_{static}}{(\rho_{ref} g)} \quad (2)$$

where P_{static} = Hydrostatic pressure at major feed zone (Pa);
ρ_{ref} = Density of pumped medium at feed zone formation temperature (kg/m^3);
g = acceleration due to gravity (m/s^2).

2.7 Production capacity and pump intake pressure

The production capacity was estimated to be in the range 15-60 kg/s. The pump intake pressure, commonly referred to as net positive suction head required ($NPSH_R$), is determined from pump curve performance curves supplied by manufacturers.

2.8 Total dynamic head required

The total dynamic head (P_D) required is calculated from equation:

$$P_D = P_S + P_H + P_f \quad (3)$$

where P_D = Total dynamic head (Pa);
P_S = Disharge head pressure (Pa);
P_H = Net water lift (Pa);
P_f = Frictional loss in the discharge tubing (Pa).

The discharge head pressure (P_S) was determined based on the required pump delivery pressure.

Net water lift, (P_H), is calculated according to equation:

$$P_H = L_H \rho_t g \quad (4)$$

where L_H = Net water lift height (m);
ρ_t = Density of pumped medium (kg/m^3);
t = Temperature of pumped medium (°C).

Net water lift height, (L_H), is calculated using equation:

$$L_H = L_V + L_N \quad (5)$$

where L_V = Water rest level in the well due to column heating (m);
L_N = Draw down in well (m).

The draw down (L_N) in a well is calculated using Equation 4, however it is assumed that drawdown is predominantly controlled by well losses and, therefore, Equation 5 is used.

$$L_N = b_D m + c_D m^2 \tag{6}$$

$$L_N = c_D m^2 \tag{7}$$

where b_D = Laminar draw down co-efficient (m/(l/s));
c_D = Turbulent draw down co-efficient (m/(l/s)^2);
m = Well total discharge (l/s or kg/s).

Friction head, (H_f), in the discharge tubing is calculated using the equation:

$$H_f = f V^2 \frac{L}{2gD_{in}} \tag{8}$$

where H_f = Friction head (m of fluid);
f = Friction factor;
V = Fluid velocity (m/s);
L = Total length of discharge tubing (m);
D_{in} = Discharge tubing pipe inner diameter (m).

The fluid velocity, (V), is calculated from the equation:

$$V = Q/\left(\frac{\pi D_{in}^2}{4}\right) \tag{9}$$

where Q = Volumetric flow rate (m^3/s).

The frictional factor, (f), is calculated based on the Reynolds number (R_e), using the Swamee – Jain equation (DiPippo, 2008) for turbulent flow:

$$Re > 5000, \qquad f = \frac{0.25}{\left[\log_{10}\left(\frac{\varepsilon}{3.7D_{in}} + \frac{5.74}{R_e^{0.9}}\right)\right]^2} \tag{10}$$

where ε = Absolute roughness.

The Reynolds number, (R_e), is calculated by the equation:

$$R_e = \frac{\rho_t D_{in} V}{\mu_t} \tag{11}$$

where μ_t = Dynamic viscosity of fluid.

Frictional loss in the discharge tubing, (P_f), is then calculated using the equation:

$$P_f = H_f \rho_t g \tag{12}$$

2.9 Pump setting depth

The pump setting depth, (L_S), is calculated from the equation:

$$L_S = L_H + h_{min} \tag{13}$$

where L_S = Pump setting depth (m);
h_{min} = minimum pump submergence (m).

The minimum pump submergence, (h_{min}), is calculated according to equation:

$$h_{min} = \frac{P_j - P_u}{\rho_t g} 10^{5+NPSH_R} + h_{fb} \quad (14)$$

where P_j = Boiling pressure of medium (bara);
P_u = Barometric pressure (bara);
$NPSH_R$ = Net positive suction head required (m);
h_{fb} = Pressure losses in bowl suction case (m).

2.10 Motor shaft power

The required motor shaft output power, (A_M), was calculated using equation:

$$A_M = A_D + A_F \quad (15)$$

where A_D = Power required by the pump unit (kW);
A_F = Total mechanical losses (kW).

Power required by the pump unit, (A_D), is calculated using the equation:

$$A_D = \frac{P_D \rho_t m 10^{-6}}{\eta_{pump}} \quad (16)$$

where η_{pump} = Pump unit efficiency.

Total mechanical losses, (A_F), in an ESP are due to mechanical losses in the motor thrust bearing (A_L). The second term in Equation 15 is, thus, omitted. In the case of LSP, mechanical losses in the shaft bearing (A_O), would have to be included as calculated in equation:

$$A_F = A_L + A_O \quad (17)$$

The power consumption, (A_N), is calculated from the equation:

$$A_N = \frac{A_M}{\eta_{motor}} \quad (18)$$

2.11 Pump type

The pump type is selected by referring to manufacturer's pump performance curves. A pump type is chosen on the basis of expected production capacity and well casing size. The selected pump should operate within its operating capacity range and close to the pump's peak efficiency.

2.12 Optimum size of ESP components

This involves determining the sizes of the ESP system components that include pump, motor and accessories. This study takes a simplified approach to ESP system components sizing by considering pump unit stages and the break horse power required by the motor in sizing the pump and motor units.

Pump stages, (Z), are determined by rounding off calculated theoretical stages to the nearest integer using manufacturer pump stage performance curves and equation:

$$Z_{theoretical} = {}^{P_D}/_{(P_I)} \quad (19)$$

where Z = Pump stages;
$Z_{theoretical}$ = Calculated theoretical stages;
P_I = Single stage head (from manufacturer pump performance curves).

The break horse power required by the pump, (BHP), is calculated from the equation:

$$BHP = Z(BHP_{stage})SG._{fluid} \quad (20)$$

where BHP = Brake horse power required by the pump;
BHP_{stage} = Brake horse power per stage (from pump performance curves);
$SG._{fluid}$ = Specific gravity of pumped medium.

3. BINARY POWER SYSTEM

Binary type energy conversion systems are typically used to exploit low temperature geothermal resources (DiPippo, 2004). Several technical variations of the binary cycle exist and include the Kalina cycle and the organic Rankine cycle (ORC). These energy conversion systems employ a secondary working fluid of a lower critical temperature and pressure in comparison with water within a closed Rankine cycle.

3.1 System components

A binary power system has two closed loops in which the primary fluid (geothermal fluid) and secondary fluid (working fluid) circulate without coming into contact. The primary fluid is produced as a pressurized liquid using one of the well flow mechanisms and is passed through heat exchangers for transfer of thermal energy to the working fluid and then injected back into the resource. The secondary fluid receives heat from the primary fluid, evaporates, expands through a turbine generating electrical power, gets cooled in a condenser and is returned to the heat exchangers by means of a feed pump. Figure 5 shows a schematic flow diagram of a proposed binary power plant. The main components include: downhole pump, sand remover, heat exchangers (preheater and evaporator), turbine, generator, air condenser and feed pump.

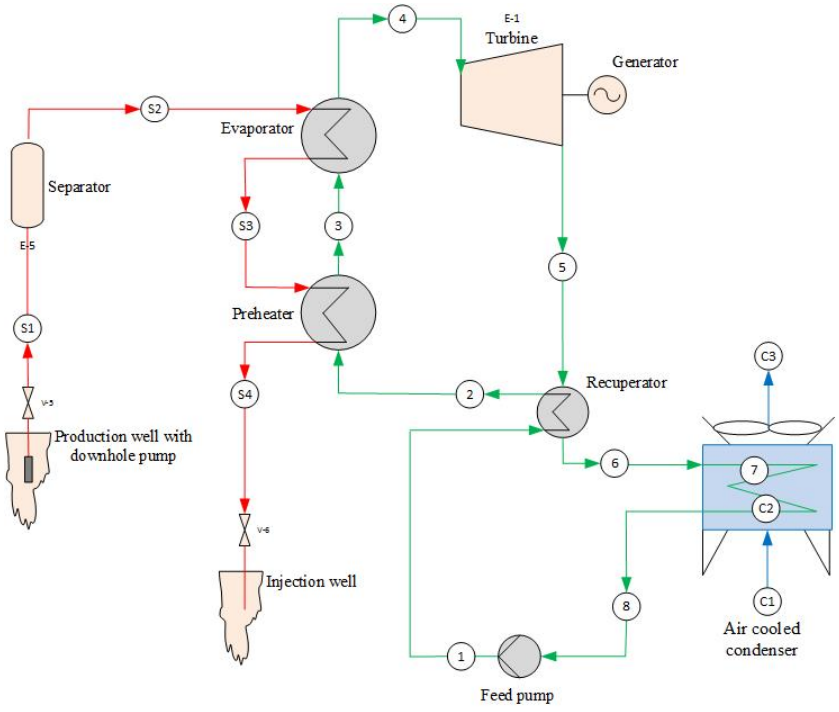

FIGURE 5: Schematic diagram of proposed binary power plant

3.2 Working fluid

Selection of the working fluid in binary power cycle is among the main considerations made. The choice has great implications on the performance of the power plant since irreversibilities associated with the heat transfer process have a negative impact on the overall efficiency of the cycle. The selection criteria for the fluid are thus based on fluid thermodynamic properties, stability of the fluid and compatibility with materials contacted, availability and cost, safety aspects and environmental impacts. Working fluids are generally classified as wet, dry or isentropic depending on the slope of the saturation vapour curve on a T – S diagram. Negative slope characterises a wet fluid; positive slope signifies dry fluid and infinite slope characterises an isentropic fluid. Findings presented by Chen et al. (2010) summarize potential working fluids. Toxicity, ozone depletion potential (ODP), global warming potential (GWP) and atmospheric life time (ALT) continue to affect the use of chlorofluorocarbons with several already phased out and others being phased out in the near future. Hydrocarbons have continued to be used with appropriate safety measures due to their flammability.

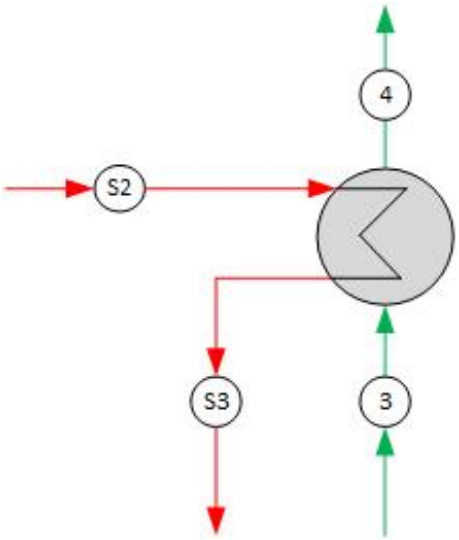

FIGURE 6: Evaporator

3.3 Binary cycle analysis

A model was set up using Engineering Equation Solver (EES) software (F-Chart Software, 2014) based on a binary power cycle as shown in Figure 5. The model was run using several working fluids to determine maximum Net power output.

3.3.1 Evaporator

Figure 6 shows the evaporator. The geothermal fluid pumped from the well goes through the sand remover and enters the evaporator via station S_2. This stream provides the heat of vaporization for the working fluid that comes as saturated liquid at evaporator pressure from the preheater and can be treated as isenthalpic, i.e. heat losses in the well and the discharge tubing are treated as negligible. Evaporation occurs from 3 to 4 along an isotherm of the working fluid. The vaporized working fluid is then fed into the turbine. The heat balance over the evaporator is given by equation:

$$Q_E = \dot{m}_{S2}(h_{S2} - h_{S3}) = \dot{m}_3(h_4 - h_3) \quad (21)$$

where Q_E = Heat transfer in the evaporator;
$\dot{m}_{S2}$ = $\dot{m}_{S1} = \dot{m}_{S3} = \dot{m}_{brine}$ = mass of geothermal fluid from the well;
$\dot{m}_3$ = $\dot{m}_1 = \dot{m}_2 = \dot{m}_4 = \dot{m}_5 = \dot{m}_6 = \dot{m}_7 = \dot{m}_8 = \dot{m}_{fluid}$ = mass of working fluid.

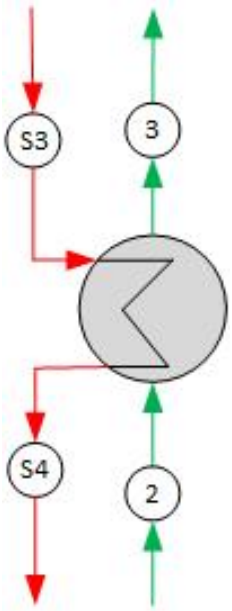

FIGURE 7: Preheater

3.3.2 Preheater

Figure 7 shows the preheater. The geothermal fluid enters via station S_3 after leaving the evaporator and leaves the evaporator at station S_4. At this stage sensible heat is added to the working fluid coming from the recuperator through station 2 to bring it to its boiling point at station 3 as it leaves the preheater. The minimum difference in temperature between the entering geothermal fluid and the leaving working fluid is known as the "pinch-point''. Heat losses in the preheater are assumed to be negligible and the heat balance over the stage is given by equation:

$$Q_{ph} = \dot{m}_{S3}(h_{S3} - h_{s4}) = \dot{m}_6(h_6 - h_8) \quad (22)$$

where Q_{ph} = Heat transfer in the preheater.

For a constant heat capacity of the fluid, the enthalpy difference in the geothermal fluid may be replaced by the temperature difference:

$$Q_{ph} = \dot{m}_{S3}c_b(T_{S3} - T_{S4}) = \dot{m}_6(h_6 - h_8) \quad (23)$$

where c_b = Specific heat capacity of the geothermal fluid at constant pressure.

3.3.3 Turbine

The turbine converts thermal energy into mechanical shaft work used to generate electricity in the generator. Figure 8 shows the turbine. Vaporised fluid enters through station 4 and exits at station 5 as vapour. The expansion process over an ideal turbine is considered isentropic and has no irreversibilities that accompany real turbines. The entropy of vaporised fluid at station 4 equals that at station 5 and subsequently the reduction in enthalpy is the largest possible. The isentropic exit enthalpy is then the enthalpy at the same entropy as that of the inlet at exit pressure as given in Equation 20.

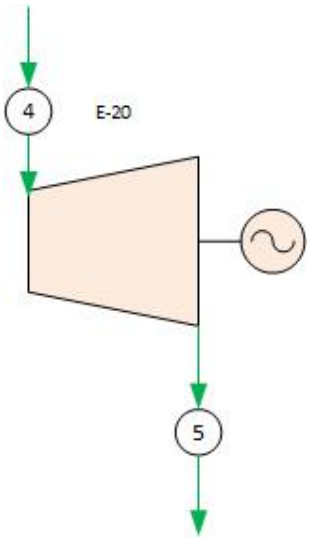

FIGURE 8: Turbine

$$h_{S5} = h(s_4, p_5) \quad (24)$$

In real turbines, irreversibilities downgrade the performance of the equipment. Reduction in enthalpy is determined by the isentropic turbine efficiency, a parameter that expresses how efficiently a real turbine approximates an idealized one as specified by the turbine manufacturer. The real turbine exit enthalpy is found using the equation:

$$\eta_t = \frac{h_4 - h_5}{h_4 - h_{S5}} \quad (25)$$

where η_t = Isentropic turbine efficiency.

Turbine work output, ($\dot{W}_t$), is thus given by the equation:

$$\dot{W}_t = m_4(h_4 - h_5) \quad (26)$$

3.3.4 Recuperator

Figure 9 shows the recuperator which is used for dry expansion type working fluid; turbine exit vapour containing extractable heat enters via station 5 and exits at station 6. The working fluid enters via station 1 and leaves through station 2. The recovery of heat helps in increasing the working fluid temperature before it enters the preheater, resulting in higher geothermal fluid exit temperature from the preheater. This leads to improved plant cycle efficiency. The heat balance over the turbine is given by the equation:

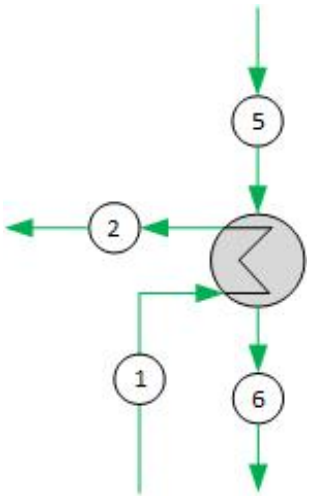

FIGURE 9: Recuperator

$$Q_R = \dot{m}_1(h_2 - h_1) = \dot{m}_5(h_5 - h_6) \quad (27)$$

3.3.5 Air cooled condenser

The condenser shown in Figure 10 is used to condense the hot working fluid from the recuperator. The working fluid enters the condenser at station 6 and leaves through station 8 as saturated liquid. Cooling air (ambient air) enters the condenser by means of suction pressure generated by fin-fans at station $C_1$and leaves at station C_3. Heat rejected by the working fluid to the air is calculated by the equation:

$$Q_C = \dot{m}_a C_a \Delta T_{cooling} = \dot{m}_6(h_6 - h_8) \qquad (28)$$

where Q_C = Heat transfer through the condenser;
$\dot{m}_a$ = Mass of air;
C_a = Specific heat capacity of air at constant pressure.

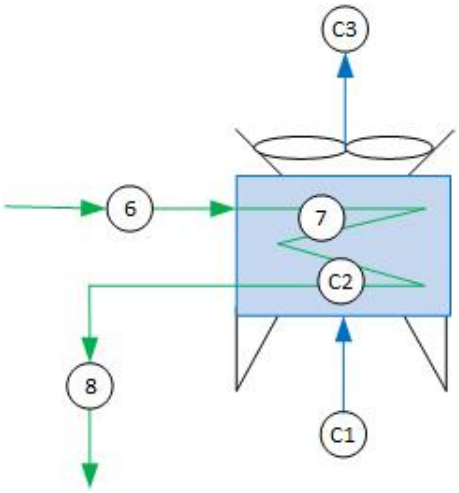

FIGURE 10: Air cooled condenser

Heat transfer from the hot working fluid to the cool air is driven by the temperature difference. It follows that the highest temperature of the cooling air must not exceed the condensation temperature in the condenser. In general, a temperature value of 5°C is used as the temperature difference between the inlet working fluid and exit cooling air temperatures. The heat balance is thus calculated by:

$$\dot{m}_a(h_{c3} - h_{c1}) = \dot{m}_{fluid}(h_6 - h_8) \qquad (29)$$

The fan power, (W_{fan}), is calculated by:

$$W_{fan} = \frac{\nu_a \Delta P}{\eta_{fan}} \qquad (30)$$

$$\nu_a = \frac{\dot{m}_a}{\rho_{a,out}} \qquad (31)$$

where ν_a = Volumetric flow rate of air (m^3/s);
ΔP = Pressure drop (Pa);
η_{fan} = Efficiency of fan;
$\rho_{a,out}$ = Density of air (kg/m^3).

3.3.6 Feed pump

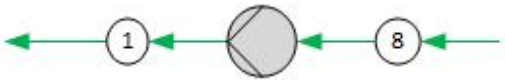

FIGURE 11: Feed pump

Figure 11 shows the pump; pump work is given by the equation:

$$W_{fp} = \dot{m}_{fluid}(h_6 - h_8) = \dot{m}_{fluid}(h_{6s} - h_8)/\eta_p \qquad (32)$$

where W_{fp} = Work done by the feed pump;
η_p = Isentropic pump efficiency.

3.3.7 Heat exchanger area

The heat transfer equipment area is calculated using equation:

$$Q = UA(LMTD) \qquad (33)$$

$$\text{LMTD} = \frac{\left(\text{T}_{\text{hot,in}} - \text{T}_{\text{cold,out}}\right) - \left(\text{T}_{\text{hot,out}} - \text{T}_{\text{cold,in}}\right)}{\ln\left[\frac{\text{T}_{\text{hot,in}} - \text{T}_{\text{cold,out}}}{\text{T}_{\text{hot,out}} - \text{T}_{\text{cold,in}}}\right]} \tag{34}$$

where Q = Heat transfer through equipment (J or kJ);
U = Overall heat transfer coefficient (°C/m^2);
A = Heat transfer area (m^2);
LMTD = Log mean temperature difference (°C).

3.3.8 Assessment of binary cycle

Binary power plants are supplied with heat from a source of finite capacity. In most cases the initial brine temperature and consequent heat input are the same. Evaluation of a power plant therefore requires the use of an appropriate thermodynamic basis. The thermal efficiency, ($\text{n}_{\text{th,I}}$), of a binary power plant can be carried out according to the first law of thermodynamics, given as:

$$\text{n}_{\text{th(I)}} = \frac{\text{W}_{\text{net}}}{\text{Q}_{\text{in}}} \tag{35}$$

$$\text{W}_{\text{net}} = \text{W}_{\text{t}} - \text{W}_{\text{parastic load}} \tag{36}$$

$$\text{W}_{\text{parasitic load}} = \text{W}_{\text{feed pump}} + \text{W}_{\text{fan}} + \text{W}_{\text{downhole pump}} \tag{37}$$

where W_{net} = Net power output;
Q_{in} = Thermal heat energy supplied to the binary system;
$\text{W}_{\text{parastic load}}$ = Power consumption by auxiliary binary plant equipment;
$W_{feed\ pump}, W_{fan}, W_{downhole\ pump}$ = feed pump, fan and dowhole pump power.

The second law (or exergetic) efficiency relates to the maximum power (or work) output that can theoretically be obtained from a system, relative to its surrounding environment. Two approaches exist, namely "brute-force" and "functional" defined as follows:

- A brute-force exergy efficiency is the ratio of the sum of all output exergy terms to the sum of all input exergy terms.
- A functional exergy efficiency is the ratio of the exergy associated with the desired energy output to the exergy associated with the energy expended to achieve the desired output.

In DiPippo and Marcille (1984) the exergetic efficiency, ($\text{n}_{\text{th,II}}$), concept when applied to a power plant simplifies to the ratio of net power output to the exergy of the motive fluid serving as the energy source for the plant. The exergetic efficiency is given by:

$$\text{n}_{\text{th(II)}} = \frac{\text{W}_{\text{net}}}{\text{E}_{\text{in}}} \tag{38}$$

$$\text{E}_{\text{in}} = \text{m}_{\text{geo fluid}}\left(\text{e}_{\text{geo fluid,in}}\right) \tag{39}$$

$$\text{e} = \text{h}_r - \text{h}_{\text{o}} - \text{T}_{\text{o}}(S_r - \text{S}_{\text{o}}) \tag{40}$$

where E_{in} = Exergy of motive fluid inflow stream;
$\text{m}_{\text{geo fluid}}$ = Mass flow rate of geothermal fluid inflow stream;
$\text{e}_{\text{geo fluid,in}}$ = Specific exergy of motive fluid inflow stream;
h = Specific enthalpy of fluid stream;
S = Specific entropy of fluid stream;
r = Set of reference motive source fluid conditions (temp. and pressure states);
o = State of ambient (dead state) conditions (temperature and pressure).

4. WELL MW-17 UTILIZATION SCHEME CALCULATIONS

The utilization scheme calculations are divided into downhole pump performance and binary power plant model calculations. In this utilization scheme the wellhead discharge pressure is assumed to be 7 bar.

4.1 Downhole pump selection and performance calculations

4.1.1 Basic data

The main feed zone is assumed to be at the depth interval of 1000 – 1200 m. Density variations due to temperature elevation are limited to the determination of the water rest level in the well due to column heating calculations. Tables 2 and 3 give basic data used in the downhole pump system design.

TABLE 2: Well MW-17 casing data

Section	Setting depth (meters RT)	Open hole diameter (inches)	Casing outer diameter (inches)	Wall thickness (inches)	Nominal weight (Pound Per Foot - PPF)
Surface	68.37	26	20	0.438	94
Intermediate/Anchor	402.73	17 1/2	13 3/8	0.380	54.5
Production	1004.57	12 1/4	9 5/8	0.472	47
Liners landing	2212.00	8 1/2	7	0.362	26

TABLE 3: Material properties

Parameter	Value/Specification
Wellhead/Master valve	ANSI class 600
Discharge tubing internal diameter	3 inches
Commercial steel pipe internal roughness	0.045mm
Fluid density	1000 kg/m^3

4.1.2 General assumptions

Engineering Equation Solver (EES) software was used for the design model of the downhole pump. The following assumptions were made.

- The static water rest level in the well is taken to be at 450 m;
- Drawdown is dominated by well losses;
- Geothermal fluid properties are comparable to water thermodynamic properties;
- No challenges (abrasion, deposition, and corrosion, temp) due to fluid chemistry are anticipated;
- Pressure losses in bowl unit (h_{fb})are negligible;
- The fluid is pumped at a temperature of 150°C;
- The pump is operated at full load; and
- SI units are used in all calculations.

4.1.3 Water rest level in well due to column heating

The water column due to well heating was calculated according to Equations 1 and 2 for two cases:

1. Partial heating of water column to pumping conditions from a depth of 1200 m upwards
2. Total heating of entire water column to pumping conditions.

Table 4 shows possible water column rise for the two cases.

TABLE 4: Initial water column rise

Effect	Static water rest level (m)	Water rest level in well due to well heating (m)	Column rise (m)
Partial heating of column	450	378	72
Total heating of column		352	98

The calculated column rise was found to be between 70 and 100 m. The rise corresponds to a water rest level in the well due to column heating in the range 350 -380 m at the onset of pumping before drawdown effects are felt. The ANSI class 600 wellhead is thus sufficient to hold the pump system discharge pressure at the onset of pumping.

4.1.4 Pump design results

The pump setting depth and total dynamic head were calculated based on a likely total well discharge mass flow in the range 15 – 60 kg/s. Table 5 shows results of the pump calculations.

The pump setting depths are in the range 436 – 529 m for the range of production capacity. Total dynamic head is calculated and varies from 46 to 61 bar while the motor power consumption is between 185 and 976 kW.

TABLE 5: Pump setting depth and total dynamic head calculations

Parameter		Values									
Mass flow	(kg/s)	15	20	25	30	35	40	45	50	55	60
Pump setting depth	(m)	436	441	447	455	464	474	486	499	513	529
Total dynamic head	(Bar)	46	47	49	50	51	53	55	57	59	61
Required motor shaft output power	(kW)	129	176	225	278	333	393	458	527	602	683
Motor power consumption	(kW)	185	251	322	397	476	562	654	753	860	976

4.1.5 Downhole pump sizing and accessories

ESP technology is currently limited to a maximum operating temperature of 204°C (400°F) and a maximum tandem motor power of 700 kW (974.5 HP) at 50 H_Z or 872 kW (1170 HP) at 60 H_Z. These ESP pump specifications allow production capacities from well MW-17 of up to 47 kg/s. Variable speed drives are commonly used to generate any frequency between 30 and 90 Hz (Bremner et al., 2006/07). This allows the ESP system to operate over a broader range of capacity, head and efficiency. The ESP system is thus proposed to include a variable speed drive as an accessory.

4.2 Binary power plant model calculations

4.2.1 Binary cycle conditions

The binary cycle specifications for the model are set as follows:

- Pumped brine mass flow rate = 45 kg/s
- Wellhead pressure = 7 bar
- Brine inlet temperature = 150°C
- Brine re-injection temperature = 80°C
- Assumed well enthalpy = 632.3 kJ/kg
- Isentropic efficiency of turbine (η_t) = 85%

- Efficiency of pump (η_p) = 75%
- Ambient temperature = 30 °C
- Pressure drops and heat losses in the system are neglected.

Overall heat transfer coefficients (U) of heat exchangers (Páll Valdimarsson, pers. comm.) are assumed as follows:

U = 1600 W/m^2°C for evaporator or vaporiser;
U = 1000 W/m^2°C for preheater;
U = 400 W/m^2°C for recuperator; and
U = 800 W/m^2°C for air called condenser.

Table 6 shows a summary of Menengai weather data used in the model calculations:

TABLE 6: Summary of weather data

Parameter	Maximum	Minimum	Average
Wind speed (m/s)	5.8	3.4	4.1
Relative humidity (%)	78	44	61
Dry bulb temperature (°C)	30	10	20
Barometric pressure (bar)			0.83

4.2.2 Model calculation results

A thermodynamic cycle model of the proposed binary power plant in Figure 5 was set up using Engineering Equation Solver (EES) software to enable detailed calculations. The EES code was then run using different working fluids to optimise net power output from the plant. Table 7 shows system parameters and results of isopentane, n-pentane, isobutane and n-butane.

TABLE 7: Summary of calculated power output

Working fluid	Turbine inlet pressure (bar-g)	Mass flow of working fluid (kg/s)	Gross output (kW)	Parasitic load (kW)	Net power output (kW)	ESP power (kW)	Total parasitic load (kW)	Thermal efficiency (%)
Isopentane	7	32.33	1546	713.6	831.9	654	713.6	6.2
n-pentane	6	28.74	1262	700.8	561.3	654	700.8	4.2
Isobutane	The pressure and temperature went above critical values							
n-butane	The pressure and temperature went above critical values							

Isobutane and n-butane went above their critical temperature and pressure. Results showed that isopentane gives the highest Net power output among the working fluid cycles studied. Maximum net output power of 831.9 kW was realised at a turbine inlet pressure of 7 bar and yielded a 6.2% thermal efficiency when considered on the basis of first law of thermodynamics. The parasitic load of the proposed plant is approximately 714 kW, majorly being load due to the ESP. Figures 12 and 13 show plots of Net power output against turbine inlet pressure for isopentane and n-pentane, while Figure 14 shows the proposed binary power plant cycle (isopentane) with EES values.

The proposed binary power plant undergoes the thermodynamic cycle, shown in Figures 15 and 16, in a temperature-entropy diagram and a pressure-enthalpy diagram, respectively.

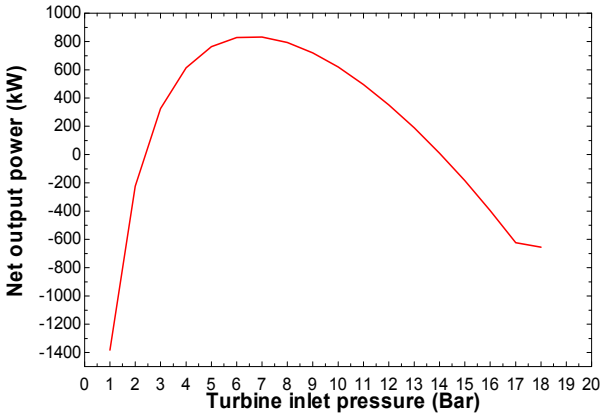

FIGURE 12: Net power output with isopentane as the working fluid

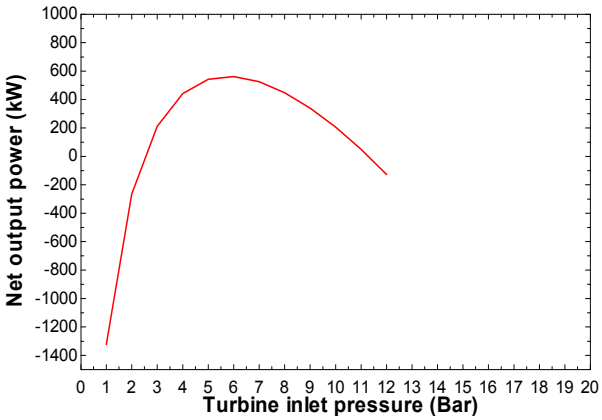

FIGURE 13: Net power output with n-Pentane as the working fluid

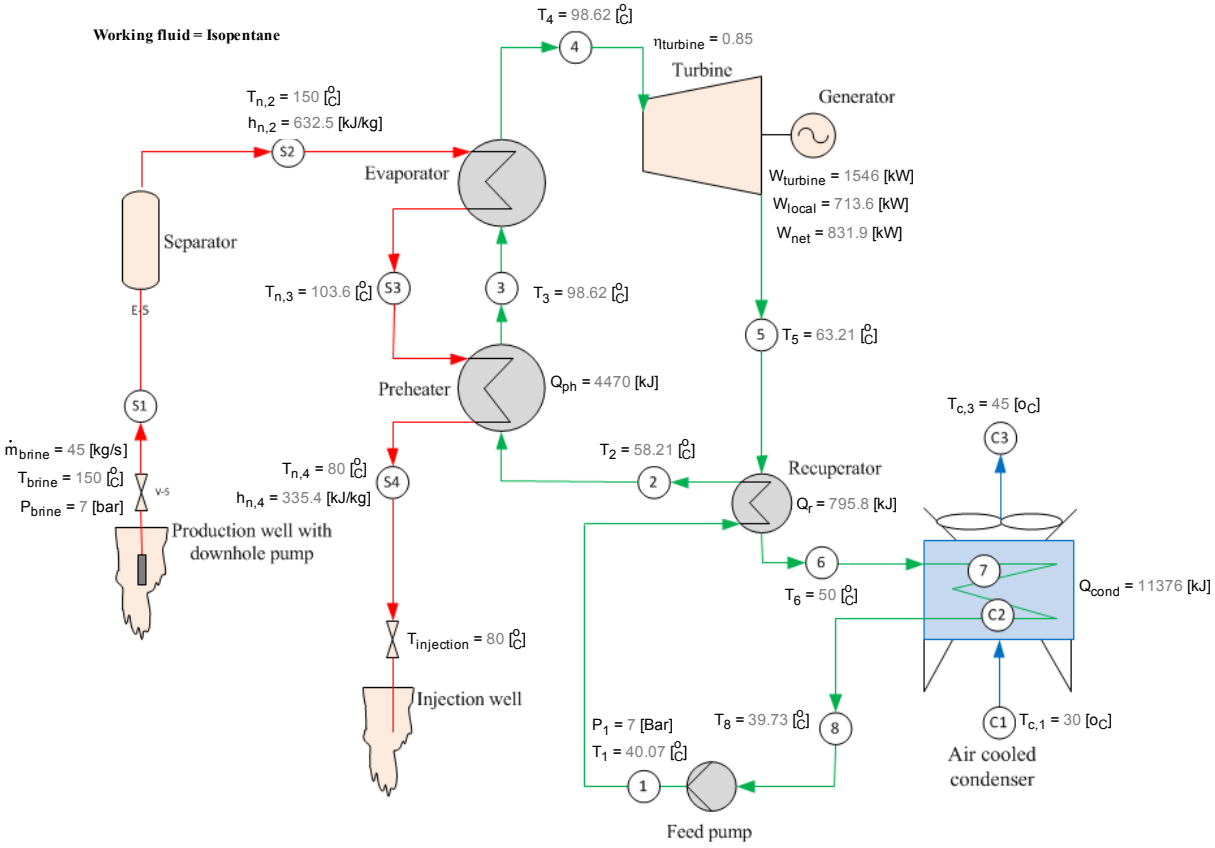

FIGURE 14: Proposed binary power plant cycle with EES values

4.3 Investment cost estimation of proposed utilization scheme

Geothermal projects are influenced by various costs which include initial investment costs, operation and maintenance costs, capital and financing costs, the costs due to economic factors and legal and regulatory costs. Calculation of initial investment can be used to give an indication of the cost of the geothermal power output. Ngugi (2012c) estimates the average installation costs in Kenya for geothermal projects is about 3.6 million US$ (2.8 million €) per MWe. The cost of the utilization scheme

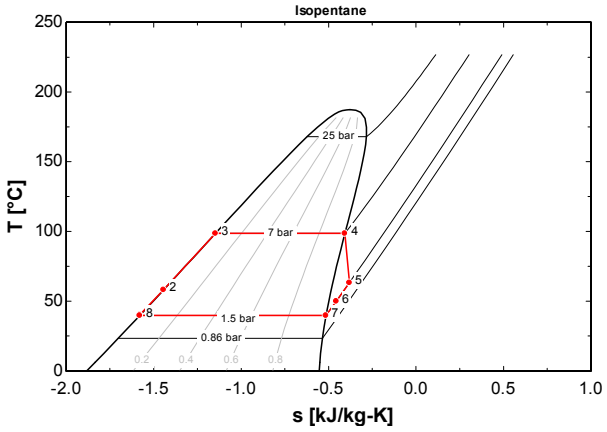

FIGURE 15: T-S diagram for proposed binary power cycle

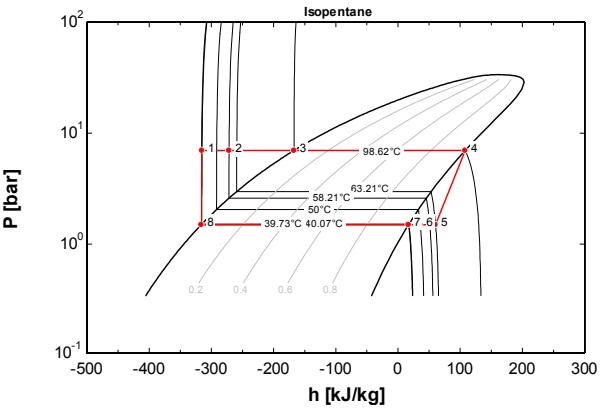

FIGURE 16: P-h diagram for proposed binary power cycle

was calculated using base costs of main plant equipment as estimated based on the experience of industry experts. In this study the costs assumed are thumb values. Table 8 shows proposed binary power plant costs based on isopentane as the working fluid.

TABLE 8: Proposed utilization scheme model based on assumed thumb values of equipment costs

S.no.	Equipment	Unit size	Basic cost / Unit size (€/m², kW)	Process heat value (kJ)	Equipment size (m², kW)	Cost of Equipment (€)
1	Preheater	m2	300	4470	391.8	117,540.00
2	Recuperator	m2	230	795.8	276.9	63,687.00
3	Air condenser	m2	265	11376	2002	530,530.00
4	Evaporator	m2	360	8896	279.3	100,548.00
5	Turbine	kW	340		1546	525,640.00
6	Feed pump	kW	500		39.54	19,770.00
Cost of mechanical equipment (35%)						1,357,715.00
Estimated binary plant cost						3,879,185.70
7	Downhole pump	kW	1000		655	655,000.00
Total estimated utilization scheme cost						4,534,185.70

The cost of mechanical equipment was assumed to represent 35% of the constructed binary plant costs (David Orn Benediktsson – Verkis Iceland, pers. comm.); this translates to a binary plant cost of 3.8 million € before considering the cost of a downhole pump. The total initial investment cost of the proposed utilization scheme is estimated at 4.5 million €.

5. CONCLUSION

Utilization of low to moderate enthalpy fluids for electrical power generation is best carried out using a binary system. This however requires careful considerations with regard to the energy conversion cycle options suitable for the project site being considered. The choice of the thermodynamic cycle working fluid ensures optimization of net power output from the plant. The proposed utilization scheme consists of a downhole electrical submersible pumping system and an organic Rankine cycle type binary power plant. The electrical submersible pump technology is currently limited to a pump capable of operating at a temperature of 204°C (400°F) and of 700 kW (974.5 HP) at 50 H_Z, maximum tandem motor power.

In this study the performance of the binary power cycle was analysed with isobutene, n-butane, isopentane and n-pentane as possible working fluids. The main conclusion is that isopentane gives the

highest net power output. The utilization scheme is ideal for early generation and would contribute to an improved exergetic efficiency of Menengai geothermal field, considering the possibility of direct use application as presented by Kinyanjui (2013).

The total investment cost of the proposed utilization scheme is estimated at 4.5 million € and translates to 5.4 million € per MWe. The proposed utilization scheme cost shows a variance of 2.6 million compared to the average Kenya installation cost of geothermal projects. The variance may be attributed to an escalation in plant equipment prices and the additional cost of a downhole pumping system.

ACKNOWLEDGEMENTS

I am profoundly grateful to my employer, Geothermal Development Company, for according me the opportunity to attend this training programme. I am also grateful to Mr. Lúdvík S. Georgsson, Director of UNU-GTP, and Mr. Ingimar G. Haraldsson, Deputy Director, for the successful organization of the programme. My sincere gratitude goes to my supervisors, Mr. Thorleikur Jóhannesson and Mr. Davíd Örn Benediktsson for their guidance, knowledge sharing and positive criticism of my work. Many thanks go to Ms. Málfrídur Ómarsdóttir, Ms. Thórhildur Ísberg and Mr. Markús A.G. Wilde for facilitating our stay and many field excursion travels. I am also thankful to the UNU Fellows for the time we shared together.

I am profoundly grateful to my family, my wife Catherine G. Wanjiru for her support and prayers, my son Nigel and daughter Hadassah for their braveness and endurance during my stay in Iceland. My heartfelt appreciation goes to my dear mother and brothers Samson and Timothy for their encouragement throughout the study period.

Thanks to Almighty God for giving me good health and wisdom.

REFERENCES

Beck, S.B., and Collins, R., 2008: *Moody diagram*. University of Sheffield, available from webpage: *en.wikipedia.org/wiki/File:Moody_diagram.jpg.*

Bremner, C., Harris, G., Kosmala, A., Nicholson, B., Ollre, A., Pearcy, M., Salmas, J.C., and Solanki, C.S., 2006/2007: Evolving technologies: Electrical submersible pumps. *Oilfield Review, 18-4* (winter 2006/2007), 30-43.

Chen, H., Goswami, D.Y., Stefanakos, E.K., 2010: A review of thermodynamic cycles and working fluids for the conversion of low-grade heat. *Renew. & Sustainable Energy Reviews, 14-9*, 3059-3067.

Culver, G.G., and Rafferty, K.D., 1998: Well pumps. In: Lienau, P.J., and Lienau, B.C. (ed), *Geothermal direct use engineering and design guidebook (3rd ed.)*. Geo-Heat Centre, Oregon Institute of Technology, Klamath Falls, OR, 211-239.

DiPippo, R., 2004: Second law assessment of binary plants generating power from low-temperature geothermal fluids. *Geothermics, 33,* 565-586.

DiPippo, R., 2008: *Geothermal power plants. Principles, applications, case studies and environmental impact*. Elsevier Ltd., Kidlington, UK, 493 pp.

DiPippo, R., and Marcille, 1984: Exergy analysis of geothermal power plants. *Geothermal Res. Council, Trans., 8,* 47-52.

Drader, D., 2011: *Improved power production efficiency of hydrothermal reservoirs using downhole pumps.* University of Iceland, MSc thesis, 60 pp.

F-Chart Software, 2014: EES, Engineering equation solver. F-Chart Software internet website, *www.fchart.com/ees/ees.shtml.*

Frost, J.A., 2004: Monitoring evaluating and optimizing down hole geothermal pump performance. *Presented at the "Down hole geothermal pump seminar", organized by Geothermal Resource Council, Indiana Wells, CA*, *Geothermal Resources Council, Transactions, 28*, 12 pp.

Genter, A., Georke, X., Graff, J., Cuenot, N., Krall, G., Schindler, M., and Ravier, G., 2010: Current status of the EGS Soultz geothermal project (France). *Proceedings of the World Geothermal Congress 2010, Bali, Indonesia*, 6 pp.

Ichikawa, S., Yasuga, H., Tosha, T., and Karasawa, H., 2000: Development of downhole pump for binary cycle power generation using geothermal water. *Proceedings of the World Geothermal Congress 2000, Kyushu - Tohoku, Japan*, 1283-1288.

Kaya, T., and Mertoglu, O., 2005: Engineering aspects of geothermal production well with down hole pumps. *Proceedings of the World Geothermal Congress 2005, Antalya, Turkey*, 8 pp.

Kinyanjui, S., 2013: Direct use of geothermal energy in Menengai, Kenya: Proposed geothermal spa and crop drying. Report 9 in: *Geothermal training in Iceland 2013*. UNU-GTP, Iceland, 109-141.

Kunaruk, U., 1991: Design and selection of deep well pumps for geothermal wells. Report 8 in: *Geothermal training in Iceland 1991*. UNU-GTP, Iceland, 51 pp.

Mibei, G., and Lagat, J., 2011: Structural controls in Menengai geothermal field. *Proceedings of Kenya Geothermal Conference*, Geothermal Association of Kenya, webpage: *www.gak.co.ke/kgc2011,* 5 pp.

Ngugi, P.K., 2012a: Kenya's plans for geothermal development – a giant step forward for geothermal. *Presented at the "Short Course on Geothermal Development and Geothermal Wells", organized by UNU-GTP and LaGeo, Santa Tecla, El Salvador*, 8 pp.

Ngugi, P.K., 2012b: Financing the Kenya geothermal vision. *Presented at "Short course on geothermal development and geothermal wells", organized by UNU-GTP and LaGeo, Santa Tecla, El Salvador,* 11 pp.

Ngugi, P.K., 2012c: What does geothermal cost? – The Kenya experience. *Presented at ''Short course VII on exploration for geothermal resource'', organized by UNU-GTP, GDC and KenGen, Naivasha, Kenya,* 13 pp.

Ofwona, C.O., Kipyego, E.K., and Suwai, J.J., 2011: Preliminary well test data of Menengai exploration wells. *Proceedings of the Kenya Geothermal Conference 2011, Nairobi*, Geothermal Association of Kenya, webpage: *www.gak.co.ke/kgc2011*, 4 pp.

Sanyal, S.K., Murrow, J.W., and Butler, S.J., 2007: Net power capacity of geothermal wells versus reservoir temperature – A practical perspective. *Proceedings of the 32nd Workshop on Geothermal Reservoir Engineering, Stanford University, Stanford, CA,* 7 pp.

Suwai, J.J., 2011: Preliminary reservoir analysis of Menengai geothermal field exploration wells. Report 32 in: *Geothermal Training in Iceland 2011*. UNU-GTP, Iceland, 799-826.

APPENDIX I: Wells MW-5A and MW-17 downhole profiles

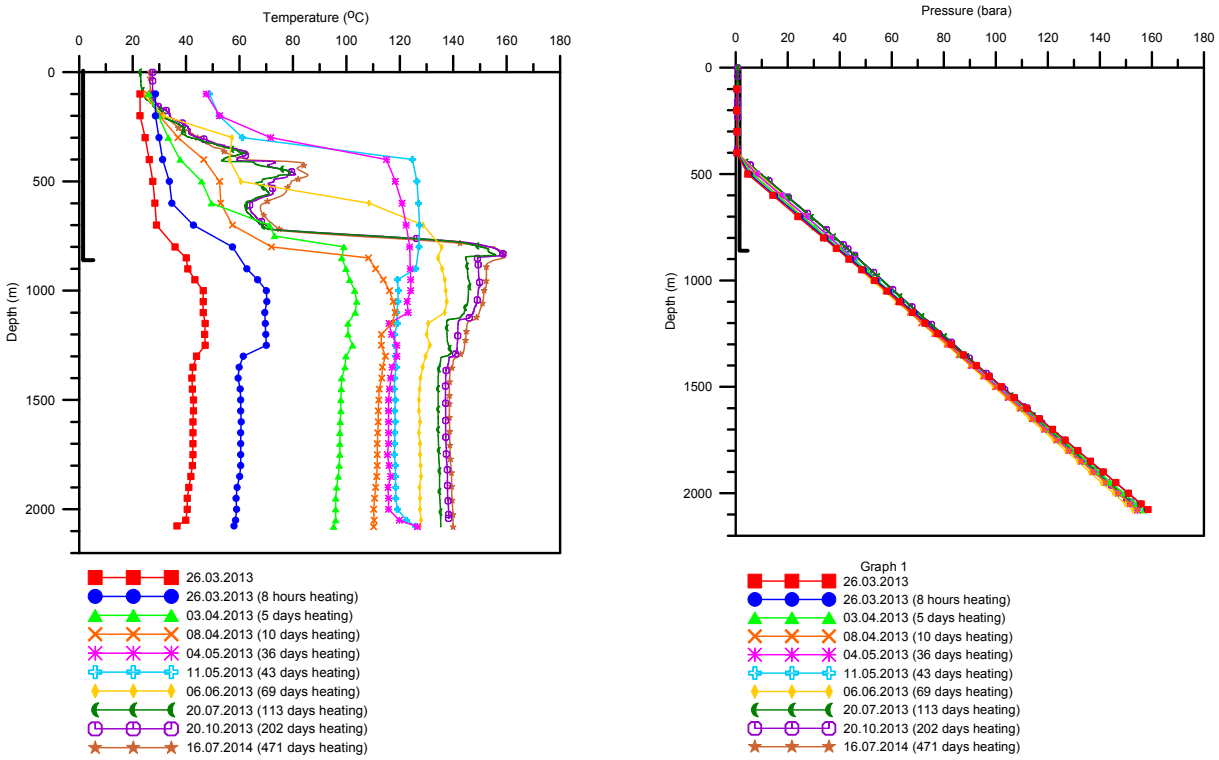

FIGURE 1: MW-5A measured temperature profiles on the left and pressure profiles on the right

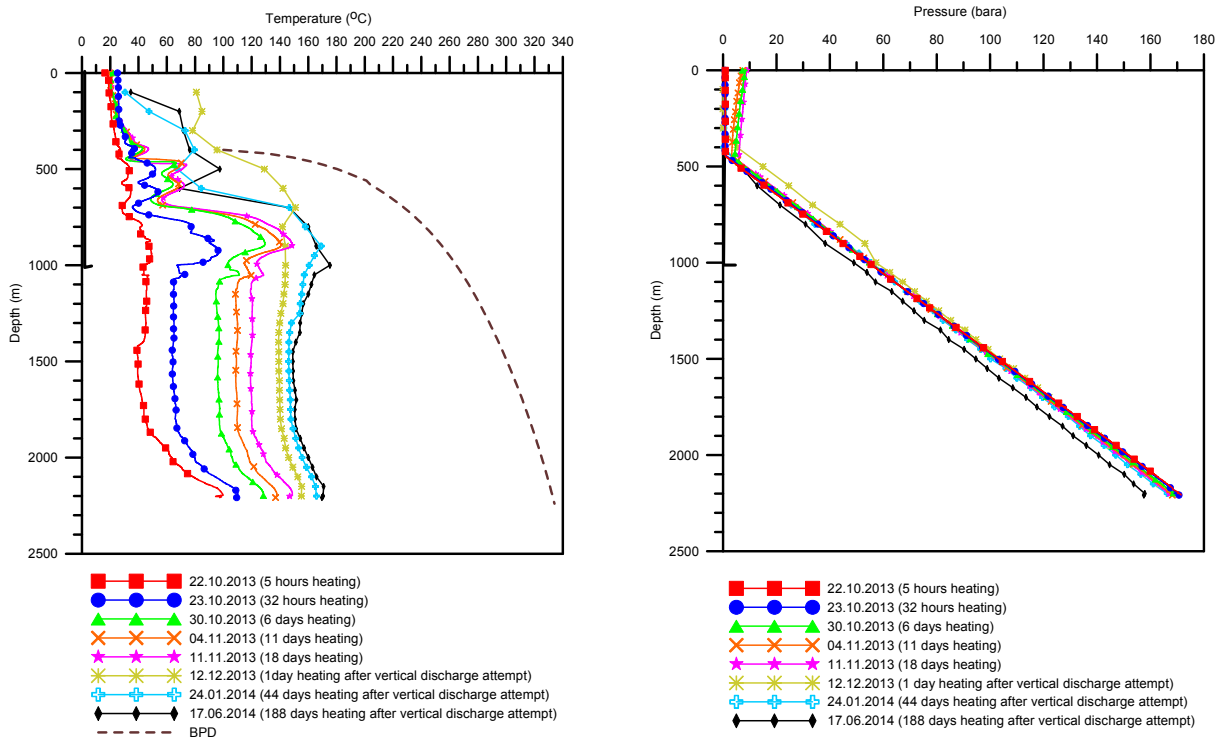

FIGURE 2: MW-17 measured temperature profiles on the left and pressure profiles on the right

APPENDIX II: Moody diagram (Beck and Collins, 2008)

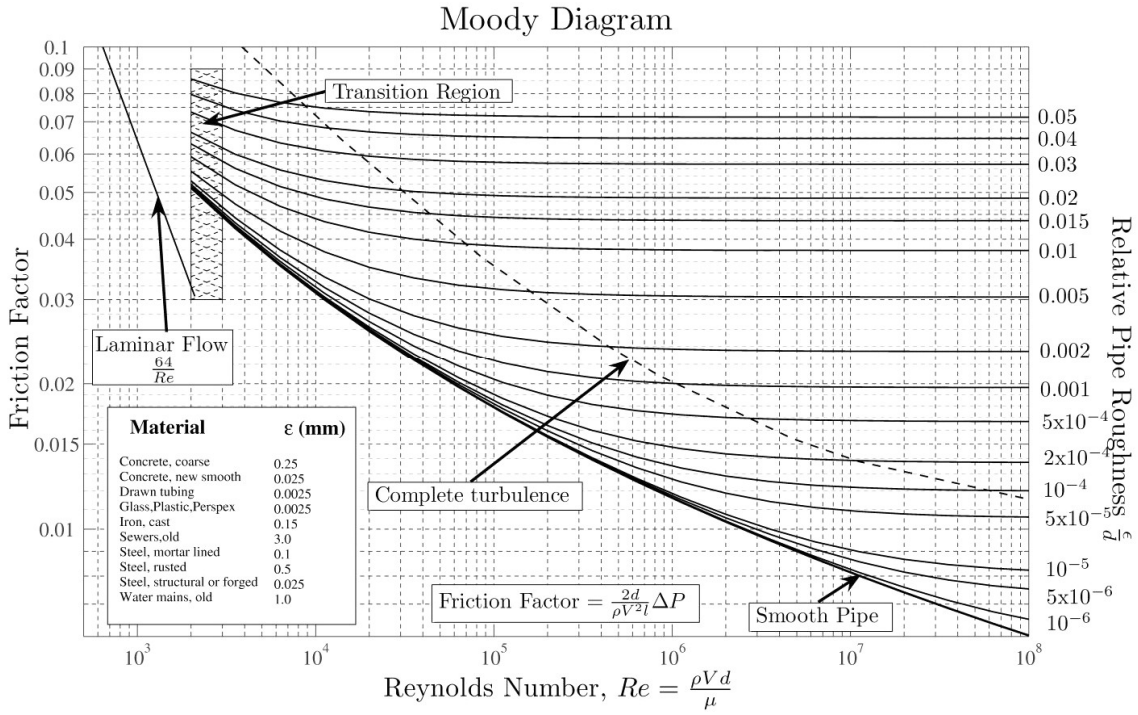

APPENDIX III: An example of EES detailed calculations run

"#######PROPOSED BINARY POWER CYCLE ANALYSIS##############Isopentane run###############Hilary R. M. Mwawasi, UNU 2014#######Optimised run#######"

"Cycle conditions"

eta_turbine=0.85
eta_pump=0.75
P_cond=1.5 "bar"
P_atmospheric=0.83 "bar"
T_ambient=30 "^o_C"
P_brine=7 "bar"
T_brine=150 "^o_C"
T_injection=80 "^o_C"
C_p_brine=Cp(Water,T=T_brine,P=P_brine) "kJ/kg,degC"
m_dot_brine=45 "kg/s"

"Well conditions"

m_dot_well=m_dot_brine "kg/s"
P_well=P_brine "bar"
T_well=T_brine "^o_C"
h_well=Enthalpy(Steam_IAPWS,T=T_well,x=0) "kJ/kg"
s_well=Entropy(Steam_IAPWS,T=T_well,x=0)" kJ/kg"

"Station 1"

m_dot_n[1]=m_dot_well
P_n[1]=P_well
T_n[1]=T_well
h_n[1]=Enthalpy(Water,T=T_n[1],P=P_n[1])
s_n[1]=Entropy(Water,T=T_n[1],P=P_n[1])

"Station 2"

m_dot_n[2]=m_dot_n[1]
T_n[2]=T_n[1]
P_n[2]=P_n[1]
h_n[2]=h_n[1]
s_n[2]=s_n[1]

"Evaporator"
"Pinch-point = 5 degC"

Q_e=m_dot_[3]*(h[4]-h[3]) "kJ"
"m_dot_n[2]*(h_n[2]-h_n[3])=m_dot_[3]*(h[4]-h[3])"
m_dot_[3]=(m_dot_n[2]*(h_n[2]-h_n[3]))/(h[4]-h[3])
T[3]=Temperature(Isopentane,P=P[1],x=0)
P[3]=P[1]
h[3]=Enthalpy(Isopentane,P=P[1],x=0)

```
s[3]=Entropy(Isopentane,P=P[1],x=0)
T_n[3]=T[3]+5
P_n[3]=P_n[1]
h_n[3]=Enthalpy(Water,T=T_n[3],P=P_n[1])
P[4]=P[1]
T[4]=Temperature(Isopentane,P=P[4],x=1)
h[4]=Enthalpy(Isopentane,P=P[4],x=1)
s[4]=Entropy(Isopentane,P=P[4],x=1)

"Preheater"

Q_ph=m_dot_n[3]*(h_n[3]-h_n[4]) "kJ"
P[2]=P[1]
T[2]=T[5]-5
h[2]=Enthalpy(Isopentane,T=T[2],P=P[2])
s[2]=Entropy(Isopentane,T=T[2],P=P[2])
m_dot_[2]=m_dot_[3]
P_n[4]=P_n[1]
T_n[4]=T_injection
h_n[4]=Enthalpy(Water,T=T_n[4],P=P_n[4])
s_n[4]=Entropy(Water,T=T_n[4],P=P_n[4])
m_dot_n[3]=m_dot_n[2]

"Turbine"

W_turbine=m_dot_[4]*(h[4]-h[5]) "kW"
m_dot_[4]=m_dot_[3]
P[5]=P_cond
{s[5]=s[4]}
h_s[5]=Enthalpy(Isopentane,P=P[5],s=s[4])
h[5]=h[4]-(eta_turbine*(h[4]-h_s[5]))
T[5]=Temperature(Isopentane,P=P[5],h=h[5])
s[5]=Entropy(Isopentane,P=P[5],h=h[5])
m_dot_[5]=m_dot_[4]

"Recuperator"
"m_dot_1*(h_2-h_1)=m_dot_5*(h_5-h_6)"

Q_r=m_dot_[5]*(h[5]-h[6]) "kJ"
T[6]=50
P[6]=P_cond
h[6]=Enthalpy(Isopentane,T=T[6],P=P[6])
s[6]=Entropy(Isopentane,T=T[6],P=P[6])
m_dot_[6]=m_dot_[5]

"Air condensor"
"m_dot_a*(h_c3-h_c1)=m_dot_6*(h_6-h_8)"

Q_cond=m_dot_[6]*(h[6]-h[8]) "kJ"
m_dot_a=(m_dot_[6]*((h[6])-(h[8])))/((h_c[3])-
(h_c[1])) "kg/s"
h_c[3]=Enthalpy(AirH2O,T=T_c[3],r=0.61,P=P
_cond)
h_c[1]=Enthalpy(AirH2O,T=T_c[1],r=0.61,P=P
_cond)
T_c[1]=T_ambient "^o_C"
T_c[3]=45 "^o_C"
P[8]=P_cond
T[8]=Temperature(Isopentane,P=P[8],x=0)
h[8]=Enthalpy(Isopentane,T=T[8],x=0)
s[8]=Entropy(Isopentane,T=T[8],x=0)
m_dot_[8]=m_dot_[6]
W_fan=(v_dot_a*dP_fan)/(eta_fan*1000) "kW"
v_dot_a=m_dot_a/rho_air "m^3/s"
dP_fan=52 "Pa"
rho_air=Density(AirH2O,T=45,r=0.61,P=P_atm
ospheric) "kg/m^3"
eta_fan=0.7
P[7]=P_cond
T[7]=T[8]
h[7]=Enthalpy(Isopentane,T=T[8],x=1)
s[7]=Entropy(Isopentane,T=T[8],x=1)

"Feed pump"

W_pump=m_dot_[1]*((h[1])-(h[8])) "kW"
s[1]=s[8]
h_s[1]=Enthalpy(Isopentane,P=P[1],s=s[1])
h[1]=h[8]+((h_s[1])-(h[8]))/eta_pump
P[1]=7
T[1]=Temperature(Isopentane,P=P[1],h=h[1])
m_dot_[1]=m_dot_[8]

"Evaporator heat transfer area (A_e)"

A_e=Q_e/(U_e*LMTD_e) "m^2"
U_e=1.600 "kW/m^2^o_C"
LMTD_e=((T_n[2]-T[4])-(T_n[3]-
T[3]))/ln((T_n[2]-T[4])/(T_n[3]-T[3])) "^o_C"

"Preheater heat transfer area (A_ph)"

A_ph=Q_ph/(U_ph*LMTD_ph) "m^2"
U_ph=1.000 "kW/m^2^o_C"
LMTD_ph=((T_n[3]-T[3])-(T_n[4]-
T[2]))/ln((T_n[3]-T[3])/(T_n[4]-T[2])) "^o_C"

"Recuperator heat transfer area (A_r)"

A_r=Q_r/(U_r*LMTD_r) "m^2"
U_r=0.400 "kW/m^2^o_C"
LMTD_r=((T[5]-T[2])-(T[6]-T[1]))/ln((T[5]-
T[2])/(T[6]-T[1])) "^o_C"

"Air condenser heat transfer area (A_cond)"

A_cond=Q_cond/(U_cond*LMTD_cond) "m^2"
U_cond=0.800 "kW/m^2^o_C"
LMTD_cond=((T[6]-T_c[3])-(T[8]-
T_c[1]))/ln((T[6]-T_c[3])/(T[8]-T_c[1])) "^o_C"

"Thermal efficiency (eta_th)"

eta_th=(W_net*100)/Q_in "%"
W_net=W_turbine-W_local "kW"
W_local=W_fan+W_pump+W_esp "kW"
W_esp=655 "kW"

Q_in=m_dot_n[1]*(h_n[1]-h_n[4]) "kJ/kg"
```